ACS OMEGA

http://pubs.acs.org/journal/acsodf

Article

Piezoelectric Property Enhancement of PZT/Poly(vinylidenefluoride-*co*-trifluoroethylene) Hybrid Films for Flexible Piezoelectric Energy Harvesters

Jian-Xun Chen,[§] Jia-Wun Li,[§] Chih-Chia Cheng, and Chih-Wei Chiu*

Cite This: *ACS Omega* 2022, 7, 793−803

Read Online

ACCESS | Metrics & More | Article Recommendations | Supporting Information

ABSTRACT: In this study, lead zirconate titanate (PZT) ceramic particles were added for further improvement. PZT belongs to the perovskite family and exhibits good piezoelectricity. Thus, it was added in this experiment to enhance the piezoelectric response of the poly(vinylidenefluoride-*co*-trifluoroethylene) (PVDF-TrFE) copolymer, which produced a voltage output of 1.958 V under a cyclic pressure of 290 N. In addition, to further disperse the PZT particles in the PVDF-TrFE matrix, tetradecylphosphonic acid (TDPA) was synthesized and employed to modify the PZT surface, after which the surface-modified PZT (m-PZT) particles were added to the PVDF-TrFE matrix. The TDPA on the PZT surface made it difficult for the particles to aggregate, allowing them to disperse in the polymer solution more stably. In this way, the PZT particles with piezoelectric responses could be uniformly dispersed in the PVDF-TrFE film, thereby further enhancing its overall piezoelectric response. The test results showed that upon the addition of 10 wt % m-PZT, the piezoelectric coefficient of m-PZT/PVDF-TrFE 10 wt % was 27 pC/N; and under a cyclic pressure of 290 N, the output voltage reached 3.426 V, which demonstrated a better piezoelectric response than the polymer film with the original PZT particles. Furthermore, the piezoelectric coefficient of m-PZT/PVDF-TrFE 10 wt % was 27.1 pC/N. This was exhibited by maintaining a piezoelectric coefficient of 26.8 pC/N after 2000 cycles. Overall, a flexible piezoelectric film with a high piezoelectric coefficient was prepared by following a simple fabrication process, which showed that this film possesses great commercial potential.

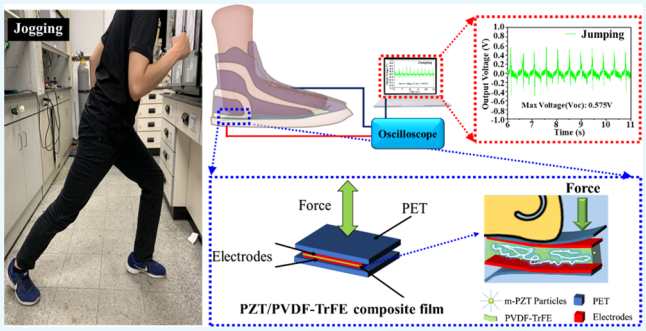

1. INTRODUCTION

With the exhaustion of fossil fuels and associated environmental issues in recent decades, energy harvesting systems have become one of the key technologies to address the energy imbalance problem.[1] At the same time, with the rapid development of portable devices, their sizes are continuously decreasing, their performances are constantly improving, and the demands for additional energy for electronic devices are also increasing.[2] Furthermore, because of the limited service life of batteries in traditional power supply devices, the need to recharge or replace the battery on a regular basis contributes to environmental pollution. Thus, alternative energy sources and the renewable energy produced by energy harvesters have received considerable attention in the scientific community.[3,4] In 1999 and 2000, researchers used polarization to improve lead zirconate titanate/vinylidenefluoride-trifluoroethylene composite,[5,6] and used polarization to increase the piezoelectric properties of ceramic and polymer composites.[7−9] Energy harvesters can reduce the planet's consumption of nonrenewable energy and alleviate the pollution caused by traditional batteries. Energy harvesters can capture energy from many different environmental sources and convert it into the required form.[10] Examples include solar energy, thermal energy, vibration energy, potential energy, kinetic energy, and other forms of mechanical energy.[11−14] Among these, vibration energy is less affected by environmental factors and has garnered widespread attention. This form of energy can be obtained from various sources, including the human body, machinery, and vehicles, as well as wind and hydropower. Piezoelectric materials can be used to capture vibration energy. These can be divided into piezoelectric single crystals, polycrystals, polymers, and composites. Among these, piezoelectric polycrystals are also referred to as piezoelectric ceramics and are known for their high dielectric and piezoelectric coefficients, high thermoelectric constants, and strong electromechanical coupling properties. However, ceramic materials also have numerous shortcomings. Compared with piezoelectric polymers, ceramics have poor mechanical

Received: September 30, 2021
Accepted: December 14, 2021
Published: December 22, 2021

https://doi.org/10.1021/acsomega.1c05451
ACS Omega 2022, 7, 793−803

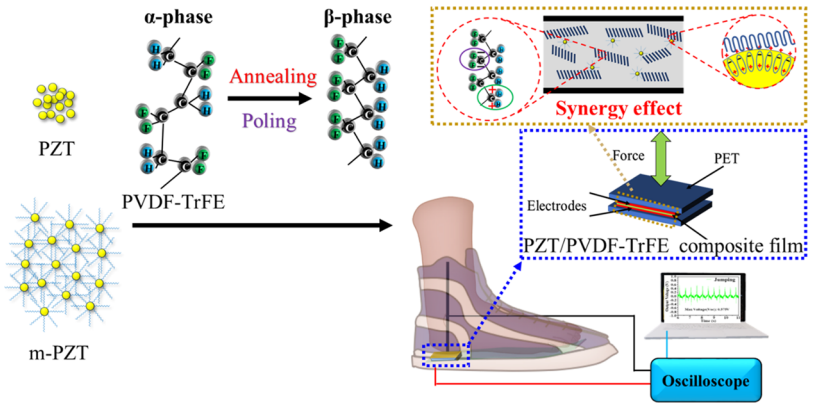

Figure 1. Design concept of PZT/PVDF-TrFE composite film and schematic diagram of the piezoelectric shoe application process.

properties, inflexibility, processing difficulty, brittleness, and nonconformity.

On the other hand, although piezoelectric polymers have relatively low dielectric and piezoelectric coefficients, they exhibit certain advantages over polycrystals, such as easy processing, flexibility, a high breakdown strength, a low density, good mechanical properties, pliability, and easy formation on different surfaces.[15−17] Because of the excellent piezoelectric response of poly(vinylidenefluoride) (PVDF) and its copolymer (poly(vinylidenefluoride-*co*-trifluoroethylene), PVDF-TrFE), PVDF piezoelectric films have been widely reported as piezoelectric materials. PVDF is a semi-crystalline polymer with properties that are directly influenced by its phase structure. There are five distinct phases in PVDF, namely, α, β, γ, δ, and ε,[18] and its piezoelectricity is determined by the formation of either the β or γ phase. Increases in the β- or γ-phase contents can therefore improve its piezoelectric effect, not only as a result of its piezoelectric and crystal structure but also because of the ease of processing the solution, low processing temperature, high sensitivity, low density, and flexibility.[19−21] Furthermore, PVDF-TrFE copolymers grafted with trifluoroethylene (TrFE) can produce the spontaneously polarized β phase. A significant number of scholars have published papers on composite piezoelectric materials in international journals in recent years. Additionally, with the rapid development of the electronics industry, piezoelectric materials are gradually being used for composites, function specialization, performance maximization, and structural miniaturization. Piezoelectric materials will be among the most important new materials in this century because of their excellent performances. The future market for electronic devices will focus on miniaturized flexible electronic devices with low power consumption. The development of piezoelectric films with excellent piezoelectric responses and low coercive voltages would therefore be advantageous. To date, however, there has been no report of successful research conducted using simple processing conditions. According to recent studies, different nanoparticles or metal halides can be added to the PVDF matrix as fillers to facilitate the formation of the β phase. These nanofillers include ZnO,[22,23] graphene oxide (GO),[24,25] carbon nanotubes (CNTs),[26] barium titanate,[27] and clay.[28,29] For instance, Liu et al. utilized multiwalled carbon nanotubes (MWCNTs) to increase the β-phase content of PVDF.[30] Chen et al.[31] incorporated $BiCl_3$ into PVDF to destroy its surrounding lattice structure with Bi^+ and Cl^- ionic states, thereby inducing the formation of the β phase. Lead zirconate titanate (PZT) is considered to be one of the most promising candidate materials because of its excellent piezoelectric and dielectric properties.[32] It has been widely reported that the piezoelectric effect can be significantly enhanced by mixing PZT particles with PVDF and electrospinning the mixture into flexible nanocomposite piezoelectric materials.[33−35] A review article on PZT and PVDF by Jain et al.[36] indicated that PZT/PVDF composites are one of the new candidate materials for energy harvesting devices, but the inhomogeneity of PZT in PVDF needs to be resolved. A comparison of the two piezoelectric polymers (i.e., PVDF vs PVDF-TrFE) showed that the dispersion of the nanomaterials could be improved more effectively when using the PVDF-TrFE copolymer, thereby promoting the formation of the β phase in PVDF (or its copolymer).[37,38] One of the effective methods for improving the dispersion of PZT in a PVDF solution is the modification of the PZT surface.[39,40] Liu et al.[41] modified PZT with 1-tetradecylphosphonic acid (TDPA) and then added the modified particles to PVDF-TrFE. Following that, they employed electrospinning to prepare a highly efficient energy harvester. To summarize, most studies have utilized electrospinning to fabricate nanocomposite piezoelectric materials. However, this fabrication approach has some drawbacks, notably needle clogging,[42] poor yield,[43] and high technical fabrication requirements.[44] As far as we know, the performance of the piezoelectric film prepared by simple blade coating has rarely been reported. Besides, the piezoelectric performance of a simple PZT modification technology in PVDF-TrFE-based composites for application in piezoelectric shoes has not been studied.

Therefore, this study utilized a simple doctor blade coating method to prepare flexible piezoelectric composites. PZT was added to PVDF-TrFE to explore the effects of different PZT contents on its piezoelectric response. Following the verification of the optimal conditions, the surface of the PZT was modified with TDPA to promote its dispersion in PVDF-TrFE. Additionally, the synergy between PZT and PVDF was utilized to enhance the piezoelectric response of PVDF-TrFE. Finally, the prepared piezoelectric composite film was packaged and applied to an energy harvesting device.

2. RESULTS AND DISCUSSION

2.1. Poly(vinylidenefluoride-*co*-trifluoroethylene) (PVDF-TrFE) Annealing Process and Polarization Treatment. In this study, the main objective was to induce the crystalline phase in the PVDF-TrFE film to form a β-phase structure through annealing and polarization treatment. Furthermore, by adding piezoelectric PZT, its synergy with

https://doi.org/10.1021/acsomega.1c05451
ACS Omega 2022, 7, 793−803

Table 1. Influence of the PVDF-TrFE Preparation Conditions on Crystallinity, β-Phase Percentage, and Piezoelectric Coefficient

sample name	applied voltage (V)	polarization time (min)	crystallinity (%)	$F(\beta)$ (%)	d_{33} (pC/N)
PVDF-TrFE	0	0	57.5	81.29	1.8 ± 0.5
PVDF-TrFE 120 °C	0	0	60.1	84.30	
PVDF-TrFE 130 °C	0	0	74.4	85.02	
PVDF-TrFE 140 °C	0	0	78.5	87.15	2.0 ± 0.8
	1000	120		78.12	2.1 ± 0.3
	2000	120		85.24	4.2 ± 0.5
	3000	120		87.03	12.6 ± 0.3
	4000	10			4.5 ± 0.5
	4000	30			8.6 ± 0.5
	4000	60			16.8 ± 0.5
	4000	120		87.50	19.3 ± 0.5
	5000	120		87.50	2.0 ± 0.8
PVDF-TrFE 150 °C	0	0	76.4	79.36	

PVDF-TrFE was utilized to improve the piezoelectric response of the final product, which was then applied to piezoelectric shoes to prepare energy harvesting components, as illustrated in Figure 1. As a result of this process, the PVDF-TrFE piezoelectric film containing m-PZT exhibited better piezoelectric properties than the original film. It was therefore necessary to determine the optimal processing conditions for the PVDF-TrFE piezoelectric film. To achieve a higher crystallinity, the PVDF-TrFE film had to be annealed, and the selected annealing temperature was above its recrystallization temperature (T_c) and below its melting temperature (T_m). In this experiment, five different annealing temperatures were used to treat the PVDF-TrFE film: no annealing, 120, 130, 140, and 150 °C. Because the paraelectric phase has higher chain mobility than the ferroelectric phase, the chain fluidity increased with temperature. The higher chain mobility favored the formation of the β phase (all-trans), which in turn enhanced the ferroelectric properties. DSC curves of PVDF-TrFE films annealed at various temperatures are shown in Figure S1. It can be observed that the melting temperature of the PVDF-TrFE film increased with the annealing temperature. When annealed at 140 °C for 1 h and then furnace-cooled to room temperature, the film's melting temperature reached 148.65 °C. On the other hand, if annealing was conducted above the melting temperature, the melting temperature of the film would decrease. Experiments showed that a higher melting temperature could be obtained when annealing at 140 °C. This was because after the annealing treatment, the molecular chains were arranged regularly. The crystallinity was enhanced, thereby leading to a higher melting temperature. Therefore, the crystallinity of PVDF-TrFE could be enhanced by the annealing treatment,[45,46] the temperature of which could also affect the phase transition of the crystal structure, and the crystallization of the ferroelectric phase in PVDF-TrFE could be improved. PVDF-TrFE should therefore be annealed at a temperature higher than the crystallization temperature (T_c). A temperature above T_c allows the molecular chains in the amorphous phase to move and rearrange into an electrically active crystalline phase, whereas when using a temperature below the melting temperature (T_m), the reorientation of lamellar chains would lead to the irreversible elimination of the ferroelectric polarization. The XRD patterns of PVDF-TrFE films annealed at various temperatures are shown in Figure S2. The experimental results demonstrated that as the annealing temperature approached the melting point (147.83 °C), the crystallinity of the PVDF-TrFE film exhibited a gradual increase. The characteristic peak of the β phase at 2θ = 20.57° gradually increased as the annealing temperature approached the melting temperature. This peak presents the reflection of the (110) and (200) planes of the crystal in the ferroelectric phase. On the other hand, the characteristic peak of the α phase at 2θ = 17.6° gradually diminished with an increase in the annealing temperature. As the annealing temperature increased above the melting temperature (T_m), the crystallinity of the PVDF-TrFE film decreased significantly. The corresponding crystallinity values are listed in Table 1. The results showed that the crystallinity of the unannealed PVDF-TrFE film was 57.5%, which increased to 78.5% after annealing at 140 °C, exhibiting an increase of 136.52%. When annealed at a temperature slightly higher than T_m, however, the crystallinity reduced. The transparency of the film gradually decreased as the annealing temperature approached the melting temperature, indicating an increase in its crystallinity (Figure S3). This phenomenon resulted from the formation of grain boundaries in the film, which scattered light, causing the film to appear foggy. the results have shown that an annealing temperature that is closer to the melting temperature causes the annealing treatment to be more effective at increasing the crystallinity of the film, this phenomenon is similar to other literature studies.[47−51] The β-phase content is the key influencing factor in a film's piezoelectric response. Therefore, this experiment used FT-IR spectroscopy for quantitative analysis. The following Lambert−Beer formula was used to calculate the β-phase contents in PVDF-TrFE films under different annealing temperatures

$$F(\beta) = \frac{X_\beta}{X_\alpha + X_\beta} = \frac{A_\beta}{\left(\frac{K_\beta}{K_\alpha}\right)A_\alpha + A_\beta} = \frac{A_\beta}{(1.26A_\alpha + A_\beta)}$$

where A_β and A_α are the areas of the characteristic peaks at 840 and 763 cm^{-1}, respectively; and K_α and K_β are the corresponding molar area coefficients, which were 6.1×10^4 and 7.7×10^4 cm^2/mol, respectively.

Figure S4 shows the FT-IR spectra of PVDF-TrFE films annealed at different temperatures. The characteristic peaks of the α phase are found at 763 and 976 cm^{-1}, and those of the β phase are found at 840 and 1401 cm^{-1}. The calculated crystallinity values are listed in Table 1. From the experimental results, it can be seen that annealing at 140 °C could increase the crystallinity of the β phase from 81.29 to 87.15%; however, annealing at 150 °C reduced the crystallinity of the β phase. This result was consistent with XRD analysis. Thus, in this study 140 °C was selected for the subsequent annealing process.

https://doi.org/10.1021/acsomega.1c05451
ACS Omega 2022, 7, 793−803

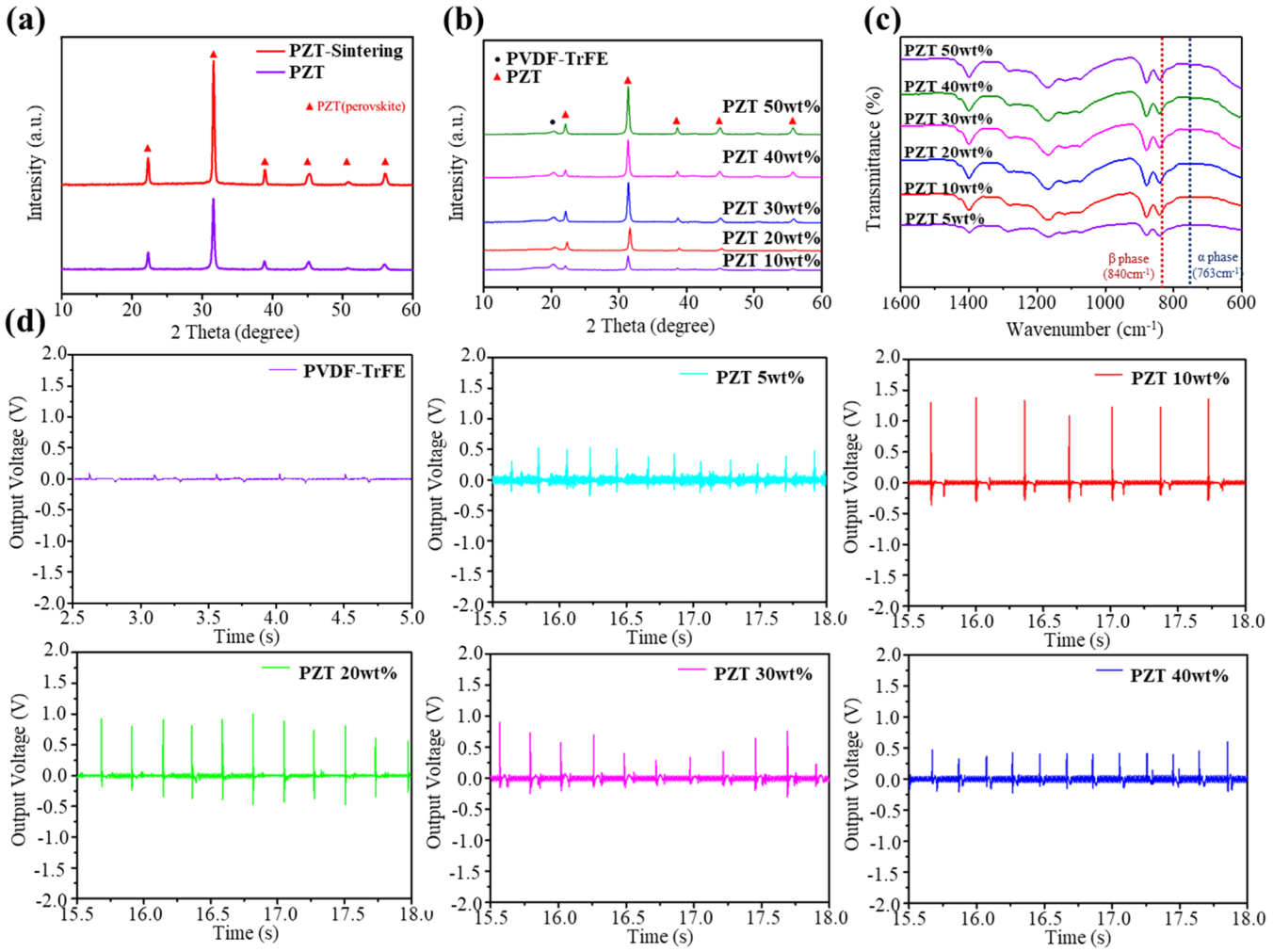

Figure 2. (a) XRD patterns of PZT and sintered PZT, (b) XRD patterns of PVDF-TrFE with different PZT contents, (c) FT-IR spectra of PVDF-TrFE with different PZT contents, and (d) open circuit output voltages of PVDF-TrFE with different PZT contents.

To further increase the β-phase content in the PVDF-TrFE film, the PVDF-TrFE film was polarized using the hot-electrode method. The hot-electrode method involves coating both the upper and lower surfaces of the film with conductive electrode materials, where the electrodes on the two sides of the film are not connected. One side of the film is connected to a positive voltage and the other side is placed on a conductive platform connected to a negative voltage to apply a high voltage to the film. In the experimental design, the film was subjected to high voltages of 1000, 2000, 3000, 4000, and 5000 V to polarize at 80 °C in silicone oil. Figure S5 shows the $P-E$ curve of the PVDF-TrFE film annealed at 140 °C. The curve converges to reach the saturation polarization voltage at ∼50 V/μm. The film thickness is ∼80 μm. Thus, it can be calculated that a voltage of ∼4000 V (50 V/μm) was required to reach saturation polarization. In addition, it can also be found that the polarization of the annealed PVDF-TrFE film has not been completed, the required polarization (P_r) value in the $P-E$ curve is relatively small.[52,53] Following this, FT-IR was used to observe the influences of different polarization voltages on the PVDF-TrFE film, as shown in Figure S6, and the corresponding β-phase contents were calculated and are presented in Table 1. According to the results, as the voltage increased, the β-phase crystallinity percentage of the PVDF-TrFE film also gradually increased. As the voltage increased to 4000 V, the β-phase crystallinity percentage was as high as 87.50%.[54] However, when the voltage was further increased to 5000 V, the β-phase crystallinity content exhibited no significant improvement compared with that at 4000 V. This was because when the applied voltage was too high, the film was susceptible to electrical breakdown, and defects would likely be formed on the material surface, thereby affecting the overall piezoelectric response of the PVDF-TrFE film. Therefore, 4000 V (a voltage below 5000 V) was selected for the subsequent polarization process in this study. The piezoelectric coefficients of PVDF-TrFE films treated under different conditions were measured using a d_{33} meter and are listed in Table 1. The d_{33} value was the number of coulombs that were generated when 1 N force was applied in the direction of the Z-axis. Thus, a larger d_{33} value indicated a better piezoelectric response. The d_{33} value is usually used as a reference for testing the piezoelectric effects of piezoelectric materials. According to the experimental results, the d_{33} value of the PVDF-TrFE film was only 1.8 ± 0.5 pC/N before annealing and increased to 2.0 ± 0.8 pC/N after annealing at 140 °C. This result showed that the annealing treatment did not significantly increase the piezoelectric coefficient. According to the experimental results, the piezoelectric coefficient increased significantly with the polarization voltage. However, polarization at 5000 V, as compared to that at 4000 V, did not significantly enhance the piezoelectric

https://doi.org/10.1021/acsomega.1c05451
ACS Omega 2022, 7, 793−803

coefficient. This observation was consistent with the saturation polarization inferred from the $P-E$ curve.

2.2. Effects of Adding Different PZT Contents to PVDF-TrFE. To increase the overall piezoelectricity of the pure PVDF-TrFE, piezoelectric ceramics were added in this study. Sintering at 1125 °C produced a better perovskite structure for the PZT piezoelectric ceramic, as shown in Figure 2a. It can be seen that after sintering, the 2θ peaks of the sintered PZT at 31° (110), 38° (111), 43° (200), and 52° (211) corresponded to the perovskite phase of PZT. The results indicated that after PZT was sintered at a high temperature, only the crystalline phase of the perovskite was present, and the characteristic peak became stronger, while no pyrochlore phase could be observed. Therefore, the annealed PZT was added to PVDF-TrFE at weight percentages of 10, 20, 30, and 40 wt %. The crystalline phase changes were examined using XRD, as shown in Figure 2b. From the results, it can be seen that the 2θ peaks at 31° (110), 38° (111), 43° (200), and 52° (211) corresponded to the perovskite phase of PZT. With an increase of the PZT content, the peak intensity of the perovskite phase gradually increased, and the peak intensity at 20.57° (200,110) corresponding to the β phase of PVDF-TrFE gradually decreased. Thus, the addition of PZT could have destroyed the β phase of PVDF-TrFE. The Lambert−Beer formula in the FT-IR method was then employed to further verify the crystalline phase changes (Figure 2c) and conduct a quantitative analysis; the results are listed in Table 2. The results confirmed that the β-phase content of the PVDF-TrFE composite film decreased with an increase in the PZT content. After annealing and polarizing pure PVDF-TrFE, its β-phase content increased to 87.5%; but with the addition of 50 wt % PZT, the β-phase content decreased to 74.93%. This may have been because the micrometer-scale PZT particles could not induce the formation of the β phase in the PVDF-TrFE composite film and might have even destroyed the β-phase structure. Figure 2d shows the output voltage signals of PVDF-TrFE with different PZT contents, and the maximum voltages are listed in Table 2. To generate the voltage signal, periodic mechanical forces were applied to the mixture, which caused a net dipole moment in the thin film element. Through this induced polarization, a potential was generated on the material, which resulted in charge carriers (electrons) flowing through an external circuit with a load to balance the electric field generated in the material. Therefore, electrical signals were generated by the piezoelectric material. Upon releasing the mechanical force, electrons gathered at the electrode and flowed back to produce a reverse signal, which immediately resulted in a decrease in potential. The results showed that the addition of PZT could increase the output voltage. The highest output voltage was reached when PZT ceramic particles were added at 10 wt %, but the voltage gradually decreased when the PZT content exceeded 10 wt %. This phenomenon could have been due to excessive aggregation during blending, which produced uneven polarization and poor dispersion of excessive PZT, ultimately resulting in poor piezoelectric responses.

Table 2. β-Phase Content and Short-Circuit Current of the Piezoelectric Composite Film

sample	PZT content (wt %)	$F(\beta)$ (%)	current (μA)	voltage (mV)
PZT/PVDF-TrFE	0	87.50	2.2	88
	5	83.71	2.6	510
	10	80.70	9.9	1372
	20	80.04	7.4	1060
	30	79.99	6.4	955
	40	78.24	2.7	670
	50	74.93		

2.3. m-PZT/PVDF-TrFE Piezoelectric Composite Film. To effectively disperse ceramic particles, the ceramics are functionalized first. Figure S7 shows a schematic diagram of how TDPA was used to modify the surface of PZT. This process mainly involved using P-OH at the end of TDPA to form a bond with the positively charged metal ion on the surface of PZT, thereby connecting the TDPA to the PZT surface. To evaluate the reaction between the TDPA and PZT, Figure S8 shows the FT-IR spectra of the PZT particles and TDPA after TDPA treatment. The absorption peak at 1630 cm^{-1} (C═O bending vibration) may represent the inorganic hydrated carbonic acid phase. The presence of bound water or absorbed water could also induce peaks. There is a peak at 1040 cm^{-1} corresponding to the P−O−M (M = surface metal) stretching vibration, which implies that TDPA was attached to the PZT surface to form a P−O bond. Figure S9 shows the XRD pattern of PZT after the surface modification with TDPA. Based on the results, it appears that m-PZT exhibited more characteristic peaks at a few angles, including peaks at 27.4 and 36.0. These two characteristic peaks indicate the presence of phosphoric acid. The XRD intensity of the PZT ceramic particles was reduced after surface modification, and a broad peak appeared. Once TDPA was combined with the PZT surface, the modified ceramic particles became loose, which could facilitate entangled interactions between random macromolecular chains. To investigate the TDPA and PZT ceramic particle surfaces, XPS was used to examine the elements present in the sample and their valence states, as shown in Figure S10a. According to the results, there was a strong peak before the modification of the PZT powder, where the binding energy corresponded to 138.23 eV of Pb 4f. However, this peak was reduced after modification with TDPA, which was caused by the grafting of phosphoric acid on the surface of the Pb element. This observation is consistent with the FT-IR result. In addition, there was little change in Zr 3d at 458.1 eV and Ti 2p at 182.46 eV after modification. A high-resolution image of the P 2p region is shown in Figure S10b. It can be seen that there was no P element peak before the modification. After the modification, the P 2p peak could be observed at 134.08 eV. A high-resolution image of the O 1s region is shown in Figure S10c. The PZT before modification showed a peak value of O 1 at 530.81 eV. Upon modification, phosphoric acid groups were introduced on the surface of the PZT ceramic particles, resulting in the presence of more oxygen elements in the m-PZT ceramic particles. These results proved that there was a strong $\pi-\pi$ interaction between adjacent molecules, and that TDPA was successfully chemically grafted onto the surface of the PZT ceramic particles.

To prepare the piezoelectric composite film (m-PZT/PVDF-TrFE), m-PZT particles were added to the PVDF-TrFE solution, as illustrated in Figure 3a. Upon TDPA modification of PZT, long alkane chains were introduced on the surface, leading to the hydrophobicity of the nanoparticles. Therefore, the particles could be dispersed more effectively in DMF in the PVDF-TrFE solution to achieve the desired dispersion effect. Furthermore, when the nanocomposite solution was coated using a doctor blade to form a film, the PZT piezoelectric ceramics exhibited a synergy effect in the PVDF-TrFE matrix, thereby increasing the overall piezoelectric response. To

https://doi.org/10.1021/acsomega.1c05451
ACS Omega 2022, 7, 793−803

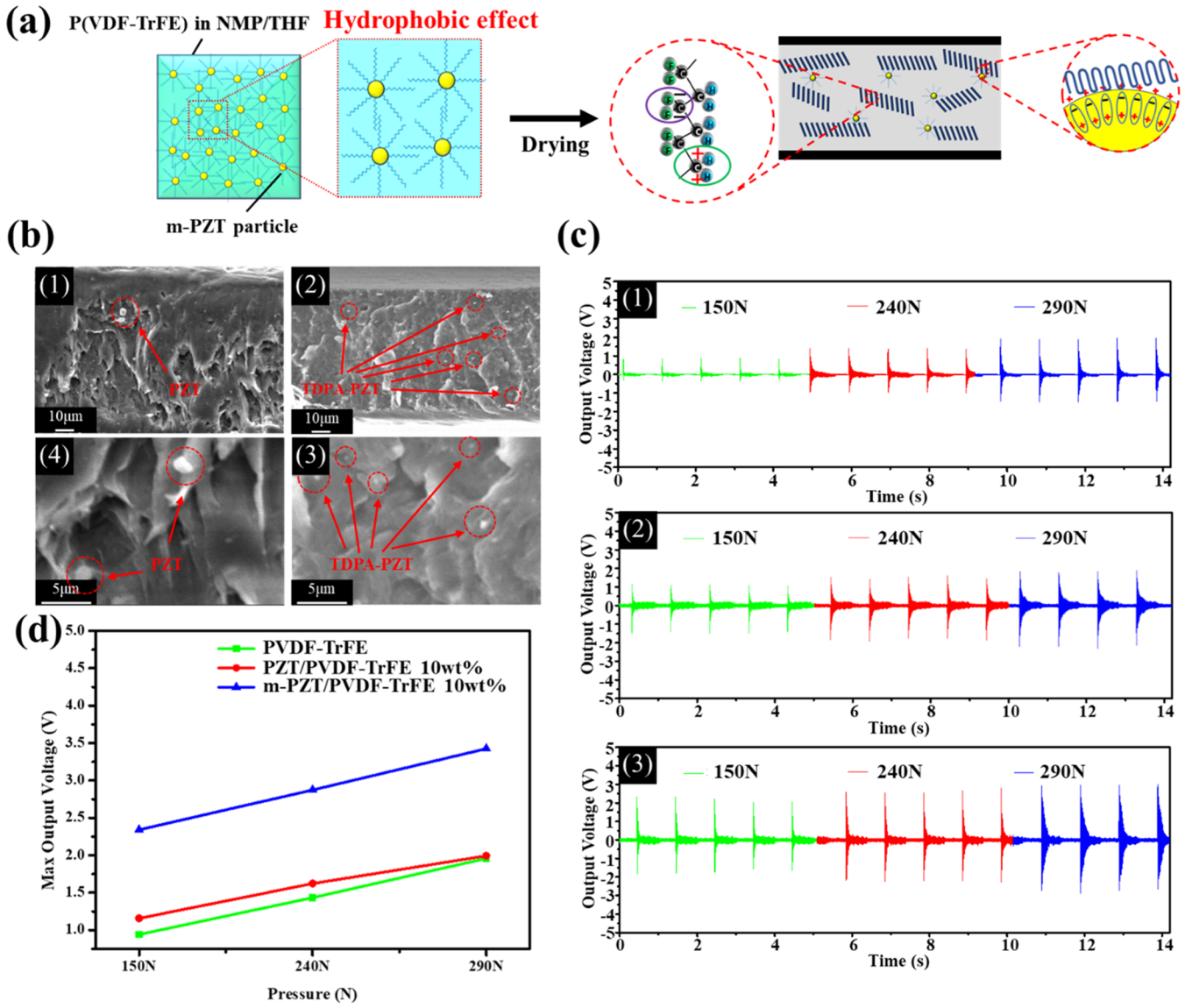

Figure 3. (a) Schematic diagram of dispersion and synergy between PZT and PVDF-TrFE; (b) cross-sectional surface morphologies of PZT/PVDF-TrFE and m-PZT/PVDF-TrFE, (1, 3) PZT/PVDF-TrFE 10 wt % and (2, 4) m-PZT/PVDF-TrFE 10 wt %; (c) output voltage of (1) pure PVDF-TrFE, (2) PZT/PVDF-TrFE, and (3) m-PZT/PVDF-TrFE; and (d) line graphs of output voltages under different cyclic pressures.

evaluate the dispersibility of the m-PZT particles in the PVDF-TrFE solution, the cross-sectional surface morphologies are shown in Figure 3b. As can be observed from the images, the agglomeration phenomenon was evident in PZT/PVDF-TrFE with the addition of 10 wt % PZT, where relatively large particles were encapsulated in the PVDF-TrFE matrix. Upon modification, the PZT particles showed significant reductions in size. This could have been because the modified PZT particles could be dispersed more effectively in the PVDF-TrFE solution and thus reduced the agglomeration effect. Figure 3c and Table 3 show the output voltages of the PVDF-TrFE, 10 wt % PZT/PVDF-TrFE, and m-PZT/PVDF-TrFE when subjected to different pressures. In all of the samples, it was observed that a higher input pressure resulted in a higher output voltage. With the addition of 10 wt % PZT and m-PZT, the piezoelectric response was significantly enhanced. The maximum output voltages of all of the samples are plotted in Figure 3d. The results show that under 290 N the maximum output voltage of pure PVDF-TrFE was 1.958 V; when 10 wt % PZT was added, the maximum output voltage increased to 1.994 V. After adding m-PZT, the film exhibited a maximum output voltage of 3.426 V under the same pressure. This was because when the original PZT was added, a synergy occurred between PVDF-TrFE and PZT, thereby improving the piezoelectric response. When PZT was modified by TDPA, its dispersion was significantly

Table 3. Maximum Output Voltages Under Different Cyclic Pressures

sample	pressure (N)	voltage (V)
PVDF-TrFE	150	0.997
	240	1.435
	290	1.958
PZT/PVDF-TrFE 10 wt %	150	1.158
	240	1.624
	290	1.994
m-PZT/PVDF-TrFE 10 wt %	150	2.342
	240	2.878
	290	3.426

https://doi.org/10.1021/acsomega.1c05451
ACS Omega 2022, 7, 793−803

improved, allowing a greater number of tiny PZT particles to be dispersed into PVDF-TrFE, resulting in a higher synergy, and thus producing the highest output voltage under all pressure conditions. The piezoelectric coefficient (d_{33}) before flexing and after 2000 cycles of flexure were compared. Table 4 and Video S1 show that the piezoelectric coefficient decreases slightly after flexure. The piezoelectric coefficient of PVDF-TrFE before flexing is 19.8 pC/N. After 2000 cycles of the flexural test, the piezoelectric coefficient dropped to 18.6 pC/N, and the piezoelectric coefficient with 10 wt % PZT was the highest. Before flexing, the piezoelectric coefficient was 22.1 pC/N, after 2000 deflection the reduction is 21.9 pC/N, the piezoelectric coefficient of the PZT modified by TDPA is 27.1 pC/N before flexing and 26.8 pC/N after flexing.

Table 4. Comparison of Piezoelectric Coefficients of PZT/PVDF-TrFE Hybrids Before and After Flexing

	before flexing d_{33} (pC/N)	after flexing d_{33} (pC/N)
PVDF-TrFE	19.8	18.6
PZT/PVDF-TrFE 10 wt %	22.1	21.9
PZT/PVDF-TrFE 20 wt %	21.8	21.5
PZT/PVDF-TrFE 30 wt %	20.9	20.4
PZT/PVDF-TrFE 40 wt %	20.2	19.8
m-PZT/PVDF-TrFE 10 wt %	27.1	26.8

2.4. Piezoelectric Shoe Applications. PET films were utilized for the element assembly of the piezoelectric composite film. Both the upper and lower layers of the piezoelectric composite film were coated with electrodes, and wires were extended, but the two layers were not interconnected. The upper and lower layers were then packaged with a PET film to enhance the mechanical properties; and hence, improve its fatigue life. To prepare piezoelectric shoes, packaged components were inserted into the insoles. By connecting the electrodes on the upper and lower layers to an oscilloscope, the voltage generated by the piezoelectric component could be recorded after being subjected to the weight of the human body. In this study, three types of films (the pure PVDF-TrFE, PZT/PVDF-TrFE, and m-PZT/PVDF-TrFE) were embedded in the insoles for jumping, walking, and jogging tests, as shown in Figure 4 and Video S1. When PVDF-TrFE was annealed and polarized, the maximum output voltages generated from jumping, walking, and jogging were 0.180, 0.09, and 0.148 V, respectively; for the PVDF-TrFE composite film with 10 wt % original PZT, the values are 0.404, 0.106, and 0.482 V, respectively; whereas the values for the PVDF-TrFE composite film with 10 wt % m-PZT were 0.575, 0.533, and 0.842 V, respectively. Based on these results, it could be concluded that the output voltage in the walking state was the lowest among all of the samples, whereas the jumping state demonstrated the highest output voltage. This result was similar to that shown in Figure 3d. This means that if the piezoelectric shoe was subjected to more pressure, it could generate a higher voltage; also, the pressure exerted on the piezoelectric shoe was the greatest when in the jumping state and the smallest in the walking state. The results also indicated that when 10 wt % of the original PZT was added to PVDF-TrFE, the maximum output voltages generated from all actions increased as a result of the synergy between the PZT and PVDF-TrFE. However, after PZT underwent surface modification it was then added to PVDF-TrFE at 10 wt %, its dispersion in PVDF-TrFE was greatly improved, generating greater synergy, and thereby increasing the maximum output voltage generated by various actions. The applicable temperature-dependent range of m-PZT/PVDF-TrFE was explored and is shown in Figure S11. When the temperature increases, the piezoelectric coefficient of the piezoelectric composite film gradually decreases. It shows a rapid decrease after 90 °C, it is completely depolarized at 150 °C, and the piezoelectric material has no piezoelectricity. Subsequently, we compared other relevant literature reports on PVDF-TrFE and sorted them in Table 5. The results show that we have used a simple process to prepare piezoelectric hybrid films with excellent piezoelectric properties.

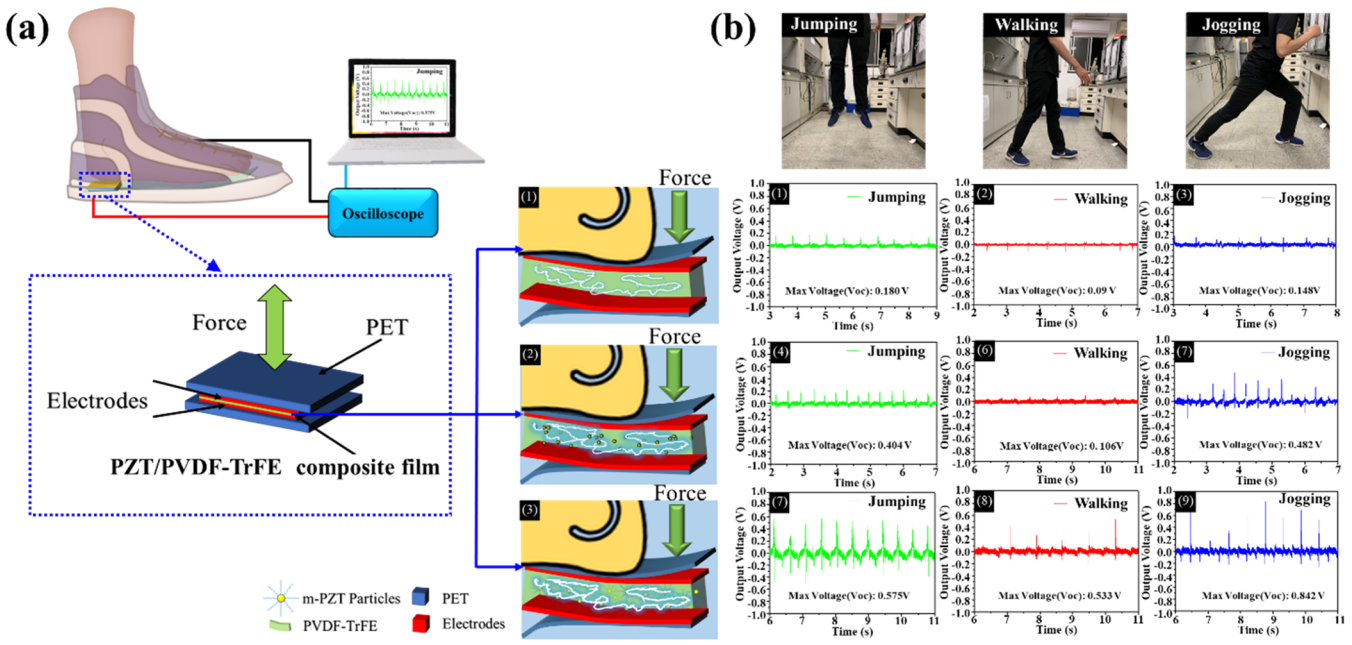

Figure 4. (a) Schematic diagram of preparation of the piezoelectric composite film element and (b) piezoelectric shoes and output voltages of (1−3) PVDF-TrFE, (4−6) PZT/PVDF-TrFE, and (7−9) m-PZT/PVDF-TrFE.

https://doi.org/10.1021/acsomega.1c05451
ACS Omega 2022, 7, 793−803

Table 5. Comparing the Performance of PVDF-TrFE-Based Generators With Those Reported in the Literature

piezoelectric materials	preparation methods	sample size (cm^2)	voltage (V)	reference
PVDF-TrFE	solution casting		1.10	55
CNT-COOH/PVDF-TrFE	solution casting		2.72	56
CaZ/PVDF-TrFE	solution casting	0.09	0.289	57
P(VDF-TrFE)	electrospinning		7	58
P(VDF-TrFE)/MWCNT	electrospinning		1.8	59
m-PZT/PVDT-TrFE 10 wt %	solution casting	1	3.426	our work

The results showed that the final product obtained using the simple doctor blade coating method in this study had a significantly improved piezoelectric response for PVDF-TrFE; thus, m-PZT/PVDF-TrFE 10 wt % could serve as a promising material for piezoelectric shoes in the future.

3. CONCLUSIONS

In this study, a PVDF-TrFE film was first annealed to increase its crystallinity and then polarized to align the microscopic dipole moments within the film, enabling it to produce a higher piezoelectric response. Experiments demonstrated that an annealing temperature of 140 °C, coupled with polarization at a voltage of 4000 V, could yield the highest β-phase content. In compression tests performed on a universal tensile testing machine, the measured output voltage of the film was 1.958 V at 290 N cyclic pressure. After that, PZT ceramic particles were added at different percentages to further enhance the film's piezoelectric response. The results demonstrated that adding PZT ceramic particles at 10 wt % could produce the best piezoelectric response, and an output voltage of 1.994 V was measured under 290 N cyclic pressure. However, because of the low dispersibility of the PZT ceramic particles, the PZT surface was modified to improve the dispersibility and stability, after which a voltage of 3.426 V was obtained under 290 N cyclic pressure. Finally, the piezoelectric film was applied to piezoelectric shoes, and good output voltages were collected, indicating that this film has great commercial potential.

4. EXPERIMENTAL SECTION

4.1. Materials. Poly(vinylidenefluoride-*co*-trifluoroethylene) copolymer (65/35 mole ratio) (PVDF-TrFE, M_w = 400 000, T_c = 127.4 °C, T_m = 148.8 °C) was purchased from Piezotech, Pierre-Benite, France. Lead zirconate titanate (PZT, model TP56) was purchased from Tcera Co., Ltd., Kaohsiung City, Taiwan. The morphologies of the powder forms of PZT were characterized by field-emission scanning electron microscopy (FE-SEM) (Figure S12) and the average particle size in DLS was 800 nm (Figure S13). Chlorotrimethylsilane (98% purity) was purchased from ACROS, NJ. Triethyl phosphate (99% purity) and 1-bromotetradecane (98% purity) were purchased from ALFA, MA.

4.2. Synthesis of Tetradecylphosphonic Acid (TDPA) and Functionalization of PZT Particles. The functional PZT ceramic particles were synthesized using the method reported in previous studies.[60−62] The commercial PZT powder was calcined at 1150 °C for 36 h to remove the polar groups and moisture absorbed on the surface of the PZT particles, as well as to induce phase formation and particle size growth. After that, the interconnected calcined PZT was ground for 4 h in a ball mill to prepare pure PZT powder. 1-TDPA was synthesized according to the Arbuzov reaction. In this reaction, 12.8 g of triethyl phosphate and 7.5 g of 1-bromotetradecane were stirred in an oil bath at 150 °C for 16 h. Then, 5 mL of distilled water, 15 mL of methanol, and 7.8 g of trimethylchlorosilane were added to the reacted solution, and the mixture was stirred in an oil bath at 60 °C for 6 h. After that, the solution was dried at 80 °C overnight to prepare TDPA. The PZT particles were added to 10 mL of ethanol, followed by the TDPA solution, which was then ultrasonically mixed for 30 min. The mixture was further stirred at 80 °C for 3 days. Next, ceramic particles were separated by centrifugation and repeatedly washed with ethanol. Finally, the washed particles were dried in an oven at 80 °C.

4.3. Preparation of the Piezoelectric Composite Film. Dimethylformamide (DMF) and methyl ethyl ketone (MEK) were mixed at a ratio of 7:3 as the solvent. The purpose of adding MEK was to reduce the boiling point of the solvent, so that the solvent could be completely volatilized below the melting point of PVDF-TrFE. After that, 20 wt % of PVDF-TrFE was added and stirred at 60 °C for 3 h with a heated stirrer to ensure dissolution and obtain the PVDF-TrFE solution. Then, the PZT powder (at weight percentages of 5, 10, 20, 30, 40, and 50 wt %) or 10 wt % surface-modified PZT (m-PZT) was added to the DMF/MEK (7:3) mixed solvent. An ultrasonic cleaner was used to physically disperse the PZT (m-PZT) particles for 30 min. The dispersed PZT (m-PZT) particles were then added to the prepared PVDF-TrFE solution to obtain the PZT/PVDF-TrFE (m-PZT/PVDF-TrFE) solution. The prepared PZT/PVDF-TrFE solution was applied to a high-temperature resistant glass by wet coating, and then placed in a vacuum oven to defoam and dry at 80 °C for 3 h to completely volatilize the solvent. The obtained PZT/PVDF-TrFE composite film had a film thickness of ∼80 μm. At this point, the crystal phase of the film was mostly the α phase without piezoelectric properties. Thus, the film exhibited no piezoelectric effect. It had to be treated with subsequent annealing and polarization processes to transform the α phase into the β phase with piezoelectric properties. The PZT/PVDF-TrFE composite film was thus placed in an oven to anneal at 140 °C for 1 h. A silver paste conductive layer was then brushed onto both sides of the annealed PZT/PVDF-TrFE film. Following this, the film was taken out and subjected to a high-voltage electric field of 4000 kV (50 V/μm) at 50 °C for 2 h of polarization to complete the preparation of PZT/PVDF-TrFE composite piezoelectric film.

4.4. Characterization and Instruments. A differential scanning calorimetry (DSC) device (model DSC 6000, Perkin Elmer) was used for DSC analysis. First, the test sample was packaged in an aluminum tray with a lid and heated at a rate of 10 °C/min to 180 °C; then, the sample was cooled at a rate of −10 °C/min to 50 °C to record the DSC curve. X-ray diffractometry (Rigaku diffractometer, BRUKER, model D2 Phaser XRD) was used to analyze the crystallinity of piezoelectric films produced under different fabrication conditions. The sample was cut into 3 × 3 cm^3 sections and then placed in a vacuum oven to dry completely. Then, the XRD test was performed in the θ range of 10−50° at a dwell time of 0.5 s per scan point. The crystallinity calculation is to integrate

https://doi.org/10.1021/acsomega.1c05451
ACS Omega 2022, 7, 793−803

the curves of the crystalline region and amorphous regions using DIFFRAC PLUS Evaluation software, and calculate the percentage of the PVDF-TrFE crystalline region. A Fourier transform infrared spectrometer (FT-IR, Digilab, Hopkinton, MA) (model (FTS-1000)) was used to identify the functional groups of the carbon material before and after modification and calculate the percentage of the β phase in the composite piezoelectric film. The nanocarbon powder and piezoelectric composite material were placed on a contact stage and scanned in a range of 400−4000 cm^{-1} at a resolution of 2 cm^{-1}. The piezoelectric coefficient (d_{33}) of the piezoelectric composite material was measured using a d_{33} meter (YE2730A, American Piezo). The polarization−electric field (P−E) curve was obtained using a TF2000 from aixACCT, (Precision LC II, Radiant Technologies, Inc.). The voltage test was performed by first cutting the sample into a voltage test pressure sheet with a diameter of 30 mm, and then tapping or testing it using a universal tensile machine (MTS-370, MTS Systems Corp.) with a compression clamp. The sample was placed between the upper and lower clamps; the loading force was configured to 150, 240, or 290 N; and the loading frequency was set to once per second. An oscilloscope (PicoScope 4224, Pico Technology Ltd., U.K.) was used to measure the voltage value generated by the composite piezoelectric film after the sample was pressed. An X-ray photoelectron spectroscopy (XPS) measurement was conducted using a Thermo Fisher Scientific (VGS) spectrometer (Waltham, MA). The Al Kα anode was used as the X-ray source (1486.6 eV), and the binding energy range of 0−1400 eV was selected for analysis. The binding energy was calibrated to the C 1s internal standard with a peak at 284.8 eV. The high-resolution C 1s spectrum was decomposed by fitting a Gaussian function to the experimental curve using nonlinear regression. A cross-section of the piezoelectric composite was frozen in liquid nitrogen to fix its structure. After that, the sample was cut and sputtered with platinum, and then observed under a high-resolution field-emission scanning electron microscope (FE-SEM), model JSM-6500F (JEOL, Tokyo, Japan).

■ ASSOCIATED CONTENT

Supporting Information

The Supporting Information is available free of charge at https://pubs.acs.org/doi/10.1021/acsomega.1c05451.

DSC curves of PVDF-TrFE films annealed at different temperatures: (a) endothermic and (b) exothermic (Figure S1); XRD patterns of PVDF-TrFE films annealed at different temperatures (Figure S2); images of PVDF-TrFE film samples annealed at different temperatures (Figure S3); FT-IR spectra of PVDF-TrFE films annealed at different temperatures (Figure S4); polarization−electric field curve of PVDF/TrFE annealed at 140 °C (Figure S5); FT-IR spectra of PVDF-TrFE films under different polarization voltages (Figure S6); schematic diagram of PZT surface modification (Figure S7); FT-IR spectra of PZT and m-PZT (Figure S8); XRD pattern of m-PZT (Figure S9); (a) XPS diagrams of PZT and m-PZT, (b) high-resolution image of the P 2p region, and (c) high-resolution image of the O 1s region (Figure S10); piezoelectric composite film of d_{33} measured at different ambient temperatures (Figure S11); FE-SEM micrographs of the powder form of PZT (Figure S12); and particle size of PZT determination by dynamic light scattering (Figure S13) (PDF)

Demonstration of m-PZT/PVDF-TrFE hybrid films were embedded in the insoles for jumping, walking, and jogging tests (Video S1) (MP4)

■ AUTHOR INFORMATION

Corresponding Author

Chih-Wei Chiu − *Department of Materials Science and Engineering, National Taiwan University of Science and Technology, Taipei 10607, Taiwan;* orcid.org/0000-0003-2258-2454; Phone: +886-2-2737-6521; Email: cwchiu@mail.ntust.edu.tw

Authors

Jian-Xun Chen − *Department of Materials Science and Engineering, National Taiwan University of Science and Technology, Taipei 10607, Taiwan*

Jia-Wun Li − *Department of Materials Science and Engineering, National Taiwan University of Science and Technology, Taipei 10607, Taiwan;* orcid.org/0000-0001-5033-2829

Chih-Chia Cheng − *Graduate Institute of Applied Science and Technology, National Taiwan University of Science and Technology, Taipei 10607, Taiwan;* orcid.org/0000-0002-1605-6338

Complete contact information is available at: https://pubs.acs.org/10.1021/acsomega.1c05451

Author Contributions

[§]J.-X.C. and J.-W.L. contributed equally to this work. Data curation, J.-X.C.; formal analysis, J.-X.C. and J.-W.L.; supervision, C.-W.C.; writing—original draft, J.-W.L. and C.-W.C.; writing—review and editing, J.-W.L., C.-C.C., and C.-W.C. All authors have read and agreed to the published version of the manuscript.

Notes

The authors declare no competing financial interest.

■ ACKNOWLEDGMENTS

This research was funded by the Ministry of Science and Technology (MOST 108-2221-E-011-042-MY2 and MOST 110-2622-E-011-028) of Taiwan.

■ REFERENCES

(1) Deka, J.; Saha, K.; Gogoi, R.; Dutta, G. K.; Raidongia, K. Fabrication of pressure-responsive energy device from nanofluidic vanadium pentoxide and polymeric hydrogel. *ACS Appl. Electron. Mater.* **2021**, *3*, 277−284.

(2) Mandal, S.; Roy, S.; Mandal, A.; Ghoshal, T.; Das, G.; Singh, A.; Goswami, D. K. Protein-based flexible moisture-induced energy-harvesting devices as self-biased electronic sensors. *ACS Appl. Electron. Mater.* **2020**, *2*, 780−789.

(3) Ghorbani, M.; Mohammadi, A.; Motezakker, A. R.; Villanueva, L. G.; Leblebici, Y.; Koşar, A. Energy harvesting in microscale with cavitating flows. *ACS Omega* **2017**, *2*, 6870−6877.

(4) Soong, Y. C.; Chiu, C. W. Multilayered graphene/boron nitride/thermoplastic polyurethane composite films with high thermal conductivity, stretchability, and washability for adjustable cooling smart clothes. *J. Colloid Interface Sci.* **2021**, *599*, 611−619.

(5) Chan, H. L.; Ng, P. K. L.; Choy, C. L. Effect of poling procedure on the properties of lead zirconate titanate/vinylidene fluoride-trifluoroethylene composites. *Appl. Phys. Lett.* **1999**, *74*, 3029−3031.

(6) Ploss, B.; Ng, W. Y.; Chan, H. L. W.; Ploss, B.; Choy, C. L. Poling study of PZT/P (VDF−TrFE) composites. *Compos. Sci. Technol.* **2001**, *61*, 957−962.

(7) Chan, H. L.; Chan, W. K.; Zhang, Y.; Choy, C. L. Pyroelectric and piezoelectric properties of lead titanate/polyvinylidene fluoride-trifluoroethylene 0-3 composites. *IEEE Trans. Dielectr. Electr. Insul.* **1998**, *5*, 505−512.
(8) Zeng, R.; Kwok, K. W.; Chan, H. L.; Choy, C. L. Longitudinal and transverse piezoelectric coefficients of lead zirconate titanate/vinylidene fluoride-trifluoroethylene composites with different polarization states. *J. Appl. Phys.* **2002**, *92*, 2674−2679.
(9) Mahdi, R. I.; Majid, W. A. Piezoelectric and pyroelectric properties of BNT-base ternary lead-free ceramic−polymer nanocomposites under different poling conditions. *RSC Adv.* **2016**, *6*, 81296−81309.
(10) Ippili, S.; Jella, V.; Eom, J. H.; Kim, J.; Hong, S.; Choi, J. S.; Yoon, S. G.; et al. An eco-friendly flexible piezoelectric energy harvester that delivers high output performance is based on lead-free $MASnI_3$ films and $MASnI_3$-PVDF composite films. *Nano Energy* **2019**, *57*, 911−923.
(11) Sultana, A.; Alam, M. M.; Ghosh, S. K.; Middya, T. R.; Mandal, D. Energy harvesting and self-powered microphone application on multifunctional inorganic-organic hybrid nanogenerator. *Energy* **2019**, *166*, 963−971.
(12) Sun, Y.; Chen, J.; Li, X.; Lu, Y.; Zhang, S.; Cheng, Z. Flexible piezoelectric energy harvester/sensor with high voltage output over wide temperature range. *Nano Energy* **2019**, *61*, 337−345.
(13) Won, S. S.; Seo, H.; Kawahara, M.; Glinsek, S.; Lee, J.; Kim, Y.; Kim, S. H.; et al. Flexible vibrational energy harvesting devices using strain-engineered perovskite piezoelectric thin films. *Nano Energy* **2019**, *55*, 182−192.
(14) Liao, M.; Ye, L.; Zhang, Y.; Chen, T.; Peng, H. The recent advance in fiber-shaped energy storage devices. *Adv. Electron. Mater.* **2019**, *5*, No. 1800456.
(15) Gebrekrstos, A.; Madras, G.; Bose, S. Piezoelectric response in electrospun poly(vinylidene fluoride) fibers containing fluoro-doped graphene derivatives. *ACS Omega* **2018**, *3*, 5317−5326.
(16) Choudhry, I.; Khalid, H. R.; Lee, H. K. Flexible piezoelectric transducers for energy harvesting and sensing from human kinematics. *ACS Appl. Electron. Mater.* **2020**, *2*, 3346−3357.
(17) Wang, Z.; Wang, X.; Sun, Z.; Li, Y.; Li, J.; Shi, Y. Enhanced energy storage property of plate-like $Na_{0.5}Bi_{4.5}Ti_4O_{15}$/poly(vinylidene fluoride) composites through texture arrangement. *Ceram. Int.* **2019**, *45*, 18356−18362.
(18) Parangusan, H.; Ponnamma, D.; AlMaadeed, M. A. A. Toward high power generating piezoelectric nanofibers: influence of particle size and surface electrostatic interaction of Ce−Fe_2O_3 and Ce−Co_3O_4 on PVDF. *ACS Omega* **2019**, *4*, 6312−6323.
(19) Lotfian, S.; Giraudmaillet, C.; Yoosefinejad, A.; Thakur, V. K.; Nezhad, H. Y. Electrospun piezoelectric polymer nanofiber layers for enabling in situ measurement in high-performance composite laminates. *ACS Omega* **2018**, *3*, 8891−8902.
(20) Carbone, C.; Benwadih, M.; D'Ambrogio, G.; Le, M. Q.; Capsal, J. F.; Cottinet, P. J. Influence of Matrix and Surfactant on Piezoelectric and Dielectric Properties of Screen-Printed $BaTiO_3$/PVDF Composites. *Polymers* **2021**, *13*, No. 2166.
(21) Pan, C. T.; Wang, S. Y.; Yen, C. K.; Kumar, A.; Kuo, S. W.; Zheng, J. L.; Wen, Z. H.; Satya, P.; Singh, R. S.; Khan, M. T.; Chaudhary, R. K.; Dai, X.; Kaushik, A. C.; Wei, D. Q.; Shiue, Y. L.; Chang, W. H. Polyvinylidene fluoride-added ceramic powder composite near-field electrospinned piezoelectric fiber-based low-frequency dynamic sensors. *ACS Omega* **2020**, *5*, 17090−17101.
(22) Rajala, S.; Schouten, M.; Krijnen, G.; Tuukkanen, S. High bending-mode sensitivity of printed piezoelectric poly-(vinylidenefluoride-co-trifluoroethylene) sensors. *ACS Omega* **2018**, *3*, 8067−8073.
(23) Choi, M.; Murillo, G.; Hwang, S.; Kim, J. W.; Jung, J. H.; Chen, C. Y.; Lee, M. Mechanical and electrical characterization of PVDF-ZnO hybrid structure for application to nanogenerator. *Nano Energy* **2017**, *33*, 462−468.
(24) Abolhasani, M. M.; Shirvanimoghaddam, K.; Naebe, M. PVDF/graphene composite nanofibers with enhanced piezoelectric performance for development of robust nanogenerators. *Compos. Sci. Technol.* **2017**, *138*, 49−56.
(25) Yuan, X.; Li, W.; Liu, H.; Han, N.; Zhang, X. A novel PVDF/graphene composite membrane based on electrospun nanofibrous film for oil/water emulsion separation. *Compos. Commun.* **2016**, *2*, 5−8.
(26) Zhang, W. B.; Zhang, Z. X.; Yang, J. H.; Huang, T.; Zhang, N.; Zheng, X. T.; Zhou, Z. W.; et al. Largely enhanced thermal conductivity of poly(vinylidene fluoride)/carbon nanotube composites achieved by adding graphene oxide. *Carbon* **2015**, *90*, 242−254.
(27) Li, Y.; Shi, Y.; Cai, F.; Xue, J.; Chen, F.; Fu, Q. Graphene sheets segregated by barium titanate for polyvinylidene fluoride composites with high dielectric constant and ultralow loss tangent. *Composites, Part A* **2015**, *78*, 318−326.
(28) Neppalli, R.; Wanjale, S.; Birajdar, M.; Causin, V. The effect of clay and of electrospinning on the polymorphism, structure and morphology of poly(vinylidene fluoride). *Eur. Polym. J.* **2013**, *49*, 90−99.
(29) Hosseini, S. M.; Yousefi, A. A. Piezoelectric sensor based on electrospun PVDF-MWCNT-Cloisite 30B hybrid nanocomposites. *Org. Electron.* **2017**, *50*, 121−129.
(30) Liu, Z. H.; Pan, C. T.; Lin, L. W.; Lai, H. W. Piezoelectric properties of PVDF/MWCNT nanofiber using near-field electrospinning. *Sens. Actuators, A* **2013**, *193*, 13−24.
(31) Chen, C.; Bai, Z.; Cao, Y.; Dong, M.; Jiang, K.; Zhou, Y.; Tao, Y.; Gu, S.; Xu, J.; Yin, X.; Xu, W. Enhanced piezoelectric performance of $BiCl_3$/PVDF nanofibers-based nanogenerators. *Compos. Sci. Technol.* **2020**, *192*, No. 108100.
(32) Gao, X.; Wu, J.; Yu, Y.; Chu, Z.; Shi, H.; Dong, S. Giant piezoelectric coefficients in relaxor piezoelectric ceramic PNN-PZT for vibration energy harvesting. *Adv. Funct. Mater.* **2018**, *28*, No. 1706895.
(33) Chamankar, N.; Khajavi, R.; Yousefi, A. A.; Rashidi, A.; Golestanifard, F. A flexible piezoelectric pressure sensor based on PVDF nanocomposite fibers doped with PZT particles for energy harvesting applications. *Ceram. Int.* **2020**, *46*, 19669−19681.
(34) Tian, G.; Deng, W.; Gao, Y.; Xiong, D.; Yan, C.; He, X.; Yang, T.; Jin, L.; Chu, X.; Zhang, H.; Yan, W.; Yang, W. Rich lamellar crystal baklava-structured PZT/PVDF piezoelectric sensor toward individual table tennis training. *Nano Energy* **2019**, *59*, 574−581.
(35) Yun, J. S.; Park, C. K.; Jeong, Y. H.; Cho, J. H.; Paik, J. H.; Yoon, S. H.; Hwang, K. R. The fabrication and characterization of piezoelectric PZT/PVDF electrospun nanofiber composites. *Nanomater. Nanotechnol.* **2016**, *6*, No. 62433.
(36) Jain, A.; Prashanth, K. J.; Sharma, A. K.; Jain, A.; Rashmi, P. N. Dielectric and piezoelectric properties of PVDF/PZT composites: A review. *Polym. Eng. Sci.* **2015**, *55*, 1589−1616.
(37) Pariy, I. O.; Ivanova, A. A.; Shvartsman, V. V.; Lupascu, D. C.; Sukhorukov, G. B.; Ludwig, T.; Bartasyte, A.; Mathur, S.; Surmenev, R. A.; Surmenev, R. A. Piezoelectric response in hybrid micropillar arrays of poly(vinylidene fluoride) and reduced graphene oxide. *Polymers* **2019**, *11*, No. 1065.
(38) Li, J. W.; Huang, C. Y.; Chen, K. Y.; Chen, J. X.; Hsu, X. Y.; Chen, Y. F.; Kuo, J. C. F.; Cheng, C. C.; Suen, M. C.; Chiu, C. W. Enhanced piezoelectric properties of poly (vinylidenefluoride-co-trifluoroethylene)/carbon-based nanomaterial composite films for pressure sensing applications. *Polymers* **2020**, *12*, No. 2999.
(39) Wang, Y.; Yao, M.; Ma, R.; Yuan, Q.; Yang, D.; Cui, B.; Ma, C.; Liu, M.; Hu, D. Design strategy of barium titanate/polyvinylidene fluoride-based nanocomposite films for high energy storage. *J. Mater. Chem. A* **2020**, *8*, 884−917.
(40) Kim, S. R.; Yoo, J. H.; Kim, J. H.; Cho, Y. S.; Park, J. W. Mechanical and piezoelectric properties of surface modified (Na, K) NbO_3-based nanoparticle-embedded piezoelectric polymer composite nanofibers for flexible piezoelectric nanogenerators. *Nano Energy* **2021**, *79*, No. 105445.
(41) Liu, K.; Choi, H. J.; Kim, B. K.; Kim, D. B.; Han, C. S.; Kim, S. W.; Kang, H. B.; Park, J. W.; Cho, Y. S. Piezoelectric energy harvesting and charging performance of $Pb(Zn_{1/3}Nb_{2/3})O_3$−$Pb(Zr_{0.5}Ti_{0.5})O_3$ nanoparticle-embedded P(VDF-TrFE) nanofiber composite sheets. *Compos. Sci. Technol.* **2018**, *168*, 296−302.
(42) Huang, C. Y.; Chiu, C. W. Facile fabrication of a stretchable and flexible nanofiber carbon film-sensing electrode by electrospinning and

https://doi.org/10.1021/acsomega.1c05451
ACS Omega 2022, 7, 793−803

its application in smart clothing for ECG and EMG monitoring. *ACS Appl. Electron. Mater.* **2021**, *3*, 676−686.
(43) Chiu, C. W.; Lin, P. H. Core/shell Ag@silicate nanoplatelets and poly(vinyl alcohol) spherical nanohybrids fabricated by coaxial electrospraying as highly sensitive SERS substrates. *RSC Adv.* **2016**, *6*, 67204−67211.
(44) Chiu, C. W.; Lin, C. A.; Hong, P. D. Melt-spinning and thermal stability behavior of TiO_2 nanoparticle/polypropylene nanocomposite fibers. *J. Polym. Res.* **2011**, *18*, 367−372.
(45) Khalifa, M.; Deeksha, B.; Mahendran, A.; Anandhan, S. Synergism of electrospinning and nano-alumina trihydrate on the polymorphism, crystallinity and piezoelectric performance of PVDF nanofibers. *JOM* **2018**, *70*, 1313−1318.
(46) Sharafkhani, S.; Kokabi, M. High performance flexible actuator: PVDF nanofibers incorporated with axially aligned carbon nanotubes. *Composites, Part B* **2021**, *222*, No. 109060.
(47) Jiang, Y.; Gong, L.; Hu, X.; Zhao, Y.; Chen, H.; Feng, L.; Zhang, D. Aligned P(VDF-TrFE) nanofibers for enhanced piezoelectric directional strain sensing. *Polymers* **2018**, *10*, No. 364.
(48) Hafner, J.; Teuschel, M.; Disnan, D.; Schneider, M.; Schmid, U. Large bias-induced piezoelectric response in the ferroelectric polymer P (VDF-TrFE) for MEMS resonators. *Mater. Res. Lett.* **2021**, *9*, 195−203.
(49) Singh, D.; Garg, A.; et al. Cooling rate controlled microstructure evolution and reduced coercivity in P (VDF−TrFE) devices for memory applications. *Org. Electron.* **2014**, *15*, 82−90.
(50) Jeong, D. G.; Ko, Y. J.; Lee, D. W.; Kwak, Y. M.; Kim, H.; Lee, K. T.; Lee, M.; Jung, J. H. Intriguing triboelectrification behavior of identical P (VDF-TrFE) polymers. *Curr. Appl. Phys.* **2021**, *29*, 122−127.
(51) Seo, J.; Son, J. Y.; Kim, W. H. Piezoelectric and ferroelectric characteristics of P (VDF-TrFE) thin films on Pt and ITO substrates. *Mater. Lett.* **2019**, *238*, 237−240.
(52) Jiang, Y. P.; Yang, T. C.; Lin, T. H.; Ho, C. M.; Chan, S. H.; Wu, M. C.; Wang, J. C. Layer-dependent solvent vapor annealing on stacked ferroelectric P (VDF-TrFE) copolymers for highly efficient nanogenerator applications. *Polymer* **2020**, *204*, No. 122822.
(53) Park, D.; Kim, M. C.; Kim, M.; Park, P.; Nah, J. Performance Enhancement of Flexible Polymer Triboelectric Generator through Polarization of the Embedded Ferroelectric Polymer Layer. *Appl. Sci.* **2021**, *11*, No. 1284.
(54) Wang, A.; Hu, M.; Zhou, L.; Qiang, X. Self-powered well-aligned P (VDF-TrFE) piezoelectric nanofiber nanogenerator for modulating an exact electrical stimulation and enhancing the proliferation of preosteoblasts. *Nanomaterials* **2019**, *9*, No. 349.
(55) Bae, J. H.; Chang, S. H. Characterization of an electroactive polymer (PVDF-TrFE) film-type sensor for health monitoring of composite structures. *Compos. Struct.* **2015**, *131*, 1090−1098.
(56) Li, J. W.; Huang, C. Y.; Chen, K. Y.; Chen, J. X.; Hsu, X. Y.; Chen, Y. F.; Kuo, C. F.; Cheng, C. C.; Suen, M. C.; Chiu, C. W. Enhanced piezoelectric properties of poly(vinylidenefluoride-co-trifluoroethylene)/carbon-based nanomaterial composite films for pressure sensing applications. *Polymers* **2020**, *12*, No. 2999.
(57) Sahoo, R.; Mishra, S.; Ramadoss, A.; Mohanty, S.; Mahapatra, S.; Nayak, S. K. An approach towards the fabrication of energy harvesting device using Ca-doped ZnO/PVDF-TrFE composite film. *Polymer* **2020**, *205*, No. 122869.
(58) Pi, Z.; Zhang, J.; Wen, C.; Zhang, Z. B.; Wu, D. Flexible piezoelectric nanogenerator made of poly (vinylidenefluoride-co-trifluoroethylene)(PVDF-TrFE) thin film. *Nano Energy* **2014**, *7*, 33−41.
(59) Wang, A.; Hu, M.; Zhou, L.; Qiang, X. Self-powered wearable pressure sensors with enhanced piezoelectric properties of aligned P (VDF-TrFE)/MWCNT composites for monitoring human physiological and muscle motion signs. *Nanomaterials* **2018**, *8*, No. 1021.
(60) Yadav, P.; Raju, T. D.; Badhulika, S. Self-poled hBN-PVDF nanofiber mat-based low-cost, ultrahigh-performance piezoelectric nanogenerator for biomechanical energy harvesting. *ACS Appl. Electron. Mater.* **2020**, *2*, 1970−1980.
(61) Zhang, C.; Fan, W.; Wang, S.; Wang, Q.; Zhang, Y.; Dong, K. Recent progress of wearable piezoelectric nanogenerators. *ACS Appl. Electron. Mater.* **2021**, *3*, 2449−2467.
(62) Soong, Y. C.; Li, J. W.; Chen, Y. F.; Chen, J. X.; Sanchez, L. W. A.; Tsai, W. Y.; Chou, T. Y.; Cheng, C. C.; Chiu, C. W. Polymer-assisted dispersion of boron nitride/graphene in a thermoplastic polyurethane hybrid for cooled smart clothes. *ACS Omega* **2021**, *6*, 28779−28787.

https://doi.org/10.1021/acsomega.1c05451
ACS Omega 2022, 7, 793−803